

DEBRIS DISK EVOLUTION AROUND A STARS

K. Y. L. SU,¹ G. H. RIEKE,¹ J. A. STANSBERRY,¹ G. BRYDEN,² K. R. STAPELFELDT,² D. E. TRILLING,¹ J. MUZEROLLE,¹
C. A. BEICHMAN,^{2,3} A. MORO-MARTIN,⁴ D. C. HINES,⁵ AND M. W. WERNER²

Received 2006 May 29; accepted 2006 August 23

ABSTRACT

We report 24 and/or 70 μm measurements of ~ 160 A-type main-sequence stars using the Multiband Imaging Photometer for *Spitzer* (MIPS). Their ages range from 5 to 850 Myr, based on estimates from the literature (cluster or moving group associations) or from the H-R diagram and isochrones. The thermal infrared excess is identified by comparing the deviation ($\sim 3\%$ and $\sim 15\%$ at the 1σ level at 24 and 70 μm , respectively) between the measurements and the synthetic Kurucz photospheric predictions. Stars showing excess infrared emission due to strong emission lines or extended nebulosity seen at 24 μm are excluded from our sample; therefore, the remaining infrared excesses are likely to arise from circumstellar debris disks. At the 3σ confidence level, the excess rate at 24 and 70 μm is 32% and $\geq 33\%$ (with an uncertainty of 5%), considerably higher than what has been found for old solar analogs and M dwarfs. Our measurements place constraints on the fractional dust luminosities and temperatures in the disks. We find that older stars tend to have lower fractional dust luminosity than younger ones. While the fractional luminosity from the excess infrared emission follows a general $1/t$ relationship, the values at a given stellar age vary by at least 2 orders of magnitude. We also find that (1) older stars possess a narrow range of temperature distribution peaking at colder temperatures, and (2) the disk emission at 70 μm persists longer than that at 24 μm . Both results suggest that the debris disk clearing process is more effective in the inner regions.

Subject headings: circumstellar matter — infrared: stars — planetary systems: formation

Online material: color figures, machine-readable table

1. INTRODUCTION

From various lines of evidence (e.g., theoretical modeling, the cratering record on the Moon, returned lunar samples, and isotopic data) it is believed that embryonic terrestrial planets in the solar system formed in ~ 10 – 30 Myr, evolved through a period of potentially immense collisions, and then underwent a reduced, but still significant, collisional period that ended with another violent episode—the Late Heavy Bombardment—at about 700 Myr (Kleine et al. 2002; Chambers 2004; Gomes et al. 2005; Strom et al. 2005). Thereafter, the system was in a relatively settled state, setting the stage for life to emerge on Earth. We are unsure whether this sequence was typical or exceptional. We are not even sure of the details of the steps because much of the evidence has been obliterated over time. Hard evidence must often be supplemented with relatively poorly tested theory to assemble a complete picture. The obvious solution would be to observe these processes as they are occurring in other planetary systems. However, observing terrestrial planets around nearby stars passing through parallel stages of evolution is virtually impossible. The planets are too dim for detection against the glare of the central stars; they are not sufficiently massive to be detected through gravitational recoil; and relatively few young stars lie close to the Sun.

However, there is a promising alternative approach: studying planetary debris disks. Debris disks arise from collisions of asteroidal (or planetesimal) bodies that lead to cascades of colli-

sions among the resulting debris. Eventually, significant amounts of this material are ground down to dust grains. Because the surface area per unit mass is large for dusty material, when these grains are heated by the central star they can produce a readily detectable level of excess emission in the mid- and far-infrared. The behavior of these infrared excesses can trace the different zones within a planetary system. The mid-IR band (*Spitzer* 24 μm , *IRAS* and *Infrared Space Observatory [ISO]* 25 μm passbands) is sensitive to grains, so long as they are around an A-type star and large enough to be in pseudostable orbits, largely between ≤ 5 and ~ 50 AU, while the far-IR band (*IRAS* and *ISO* 60 μm , *Spitzer* 70 μm passbands) is sensitive to material between ~ 50 and 200 AU. Detailed studies of the behavior of debris disks over time in these two bands can indicate how the stages deduced for the early evolution of the solar system are playing out in hundreds of other planetary systems.

Pioneering studies with *IRAS* and *ISO* suggest a systematic drop in infrared excess with stellar age (e.g., Habing et al. 2001; Spangler et al. 2001), qualitatively similar to the drop that would be deduced from the settling down of the solar system. However, because of limitations in the sensitivity and the accuracy of measurements with these two missions, they were unable to show unambiguously how debris disks evolve. *Spitzer* brings significant advances in both sensitivity and photometric accuracy, increasing our ability to detect low levels of infrared excesses around hundreds of stars. A-type stars provide an ideal laboratory to study the early stages in planetary system evolution, particularly in the zones relevant for evolution of terrestrial planets (Earth-like temperatures occur at about 5 AU from such stars). Their main-sequence lifetimes are long enough (~ 800 Myr) to encompass the entire period of interest, they are of high enough luminosity to light up their debris well, they are sufficiently abundant and bright that many can be observed readily, and they are cool enough that they are unlikely to create infrared excesses in the form of ionized gas. Rieke et al. (2005) have already conducted a study of the 24/25 μm

¹ Steward Observatory, University of Arizona, 933 North Cherry Avenue, Tucson, AZ 85721; ksu@as.arizona.edu.

² Jet Propulsion Lab, California Institute of Technology, 4800 Oak Grove Drive, Pasadena, CA 91109.

³ Michelson Science Center, California Institute of Technology, M/S 100-22, Pasadena, CA 91125.

⁴ Department of Astrophysical Sciences, Princeton University, Princeton, NJ 08540.

⁵ Space Science Institute, 4700 Walnut Street, Suite 205, Boulder, CO 80301.

excesses in such stars, based on a combination of *IRAS* and Multi-band Imaging Photometer for *Spitzer* (MIPS) measurements of stars in the field and MIPS measurements of stars in clusters. At that time, relatively few field stars had been measured well with *Spitzer* at 70 μm . In this paper, we report MIPS photometry at 24 and 70 μm of 160 main-sequence early-type stars, enough to give a much better understanding of the evolution of debris systems.

2. OBSERVATIONS AND DATA REDUCTION

2.1. Sample Selection

The majority (128) of the stars in this study are from the *Spitzer* Guaranteed Time Observation (GTO) programs (ASTAR, FAB4, and DIRTY12), for which most were selected because they had known ages based on cluster membership or association with moving groups. An additional 32 stars are included from the *Spitzer* calibration observations. In total, our sample includes 160 stars ranging in spectral type from B6 to A7, but mostly ($\sim 85\%$) from B9 to A7. We have also developed a tool to determine ages from the Hertzsprung-Russell diagram (HRD; Rieke et al. 2005), for checking consistency and estimating ages for the stars that are not in clusters or moving group associations. Two stars in the calibration programs are too bright to be observed at 24 μm , while only nine stars are bright enough at 70 μm to be observed as calibrators. Hence, a total of 158 MIPS 24 μm measurements and 137 MIPS 70 μm measurements are reported here. The AOR keys, stellar properties, and estimated ages are listed in Table 1.

Most of the stars in our sample are single stars (according to the literature and/or SIMBAD database); there are only 10 binary/multiple systems. These are either spectroscopic binaries (unresolved in ground-based optical photometry) or wide binaries with separations larger than the MIPS 24 μm beam (resolved at 24 μm). In addition, we also double checked the stars with infrared excesses (identified by the method discussed below) in the 2MASS catalog and found no nearby objects on the sky that could confuse the MIPS 24 and 70 μm measurements. Therefore, the false detection of infrared excesses due to binary components or positional coincidence is unlikely.

2.2. Data Reduction and Source Extraction

All data were processed using the MIPS instrument team Data Analysis Tool (Gordon et al. 2005) for basic reduction (dark subtraction, flat fielding/illumination correction). The known transient behaviors associated with the Ge detectors were removed by time filtering the data in the 70 μm default-scale mode and by subtracting the off-source chopped background observations for data in the 70 μm fine-scale mode. The processed data were then combined using the world coordinate system (WCS) information to produce final mosaics with pixels half the size of the physical pixel scale.

The photometry for each target was extracted using aperture photometry with multiple aperture settings, as well as point-spread function (PSF) fitting at both bands. By averaging the photometry using different methods (including multiple apertures), the estimated error provides a better estimate of the effects of image quality, background noise, and nearby contaminating sources. For aperture photometry at 24 μm , we first determined the centroid of each target by fitting a two-dimensional Gaussian core and then computed the averaged integrated flux within a large aperture (a radius of 14".94 with sky annulus between 29".88 and 42".33) and a small aperture (a radius of 6".23 with sky annulus between 19".92 and 29".88). Because the PSF at 70 μm is not well sampled and the *Spitzer* pointing is good to within 1", for aperture photometry at the 70 μm default scale we used the WCS information to place

the aperture center and then measured total flux for two different aperture settings: a large aperture (a radius of 29".55 with sky annulus between 39".40 and 68".95) and a small aperture (a radius of 15".96 with sky annulus between 18".03 and 39".01). At 70 μm fine-scale mode, we determined the centroid the same way as for the 24 μm data, but only used a single aperture (a radius of 16", with sky annulus between 19" and 39") due to the limited field of view. We determined the aperture correction based on the theoretical STinyTim PSFs (Krist 2002) that were smoothed to match the observed PSFs. An aperture correction of 1.143 (1.298) for the large aperture and 1.699 (1.972) for the small aperture was applied to the aperture photometry at 24 μm (70 μm default scale). A value of 1.933 for the 70 μm fine-scale mode was used for the aperture correction.

We used StarFinder (Diolaiti et al. 2000) to extract point-source photometry via PSF fitting. The PSF used at 24 μm was constructed based on isolated calibration stars, while at 70 μm we used the smoothed STinyTim PSFs. For bright targets without other nearby contaminating sources, the results from aperture photometry and PSF fitting agree within 1% at 24 μm and 2%–5% at 70 μm . Some stars in our sample are located in high-cirrus regions; however, the background variation at 70 μm is generally less than 10% across the whole field (5' by 2.5'). For the targets that have higher cirrus variations, we made sure that the extracted source position agrees within $\leq 1''$ (a general *Spitzer* pointing error) between 24 and 70 μm . The final measured flux and uncertainty were determined by averaging the different photometry methods. Conversion factors of 1.05×10^{-3} , 16.5, and 61.6 mJy arcsec $^{-2}$ were used to transfer measured instrumental units to physical units (mJy) for 24 μm , 70 μm default-scale, and 70 μm fine-scale modes, respectively. The absolute flux calibration errors are less than 5% at 24 μm and 10% at 70 μm (C. Engelbracht et al. 2006, in preparation; K. Gordon et al. 2006, in preparation). The errors presented here are the intrinsic noise from images and do not include the calibration errors.

At 24 μm , the majority of the stars in the sample have high ($\gg 20$) signal-to-noise ratio detections, except those that have contamination from nearby back-/foreground sources or nebulosity. For our 70 μm observations, all stars observed in the GTO ASTAR program used the default-scale photometry AOT. The integration times for these observations were planned so that they would provide at least a 1 σ detection of the photosphere (including detector and background noises), but due to various circumstances of observations and general overestimations of the *Spitzer* sensitivity, many of these sources were not detected at 70 μm . Observations from the other GTO programs (FAB4 and DIRTY12) targeted known *IRAS* debris disk candidates; therefore, the integration time was designed for high signal-to-noise detections. Finally, observations from the calibration program were aimed so that they would detect the predicted photospheres at least at the 3 σ level.

In all cases, a threshold of 3 σ was set for source detection. If the signal-to-noise ratio is less than 3, we use the 3 σ flux as an upper limit. We show in Table 1 the final measurements ($F_{m,24}$ and $F_{m,70}$ for 24 and 70 μm , respectively), uncertainties (σ_{24} and σ_{70}) and signal-to-noise ratios (S/N_{24} and S/N_{70}) for the entire sample.

2.3. Supplemental *IRAS* Sample

The stars observed with *Spitzer* were selected on the bases of (1) observability (background brightness and stellar magnitude) and (2) availability of accurate age estimates (membership in cluster or moving groups, etc.). There are a number of stars (47) that

TABLE 1
SAMPLE OF STARS AND MIPS MEASUREMENTS

Name	AOR Key	Spectral Type	Distance (pc)	Cluster/Moving Group	Age (Myr)	Age Reference	$F_{m,24}$ (mJy)	σ_{24} (mJy)	S/N ₂₄	R_{24}	IRE ₂₄	$F_{m,70}$ (mJy)	σ_{70} (mJy)	S/N ₇₀	R_{70}	IRE ₇₀
HD000319.....	3972864	A1 V	80.3	...	600	3	43.69	0.78	56.01	0.979	NO	<13.6	4.53	3	2.742	UPL
HD001160.....	10090496	A0 V	136.6	...	0 ^a	22	10.56	0.2	52.8	0.939	NO
HD002262.....	3692544	A7 V	23.5	...	690	22	304.61	4.05	75.21	1.063	YES	78.7	3.74	21.04	2.548	YES
	6036736															
	3692544															
	6036736															
HD002811.....	9940224	A3 V	205.8	...	750	22	10.56	0.07	150.86	0.95	NO
HD004150.....	3973120	A0 IV	73.7	...	325	4	139.99	2.5	56	1.041	NO	24.73	2.23	11.09	1.685	YES
HD011413.....	3973376	A1 V	74.8	...	600	3	50.73	0.91	55.75	1.034	NO	52.32	2.15	24.33	9.817	YES
HD011636.....	4228096	A5 V	18.3	...	620	5	811.52	3.28	247.41	0.961	NO	85.76	9.38	9.14	0.924	NO
HD014055.....	8796416	A1 Vnn	36.1	...	300	6	282.66	6.63	42.63	1.445	YES	787.83	157.57	5	36.377	YES
	8796160															
HD014228.....	9021952	B8 IV/V	47.5	...	115	5	185.6	1.66	111.81	0.969	NO	<41.23	13.74	3	2.033	UPL
HD014943.....	9940480	A5 V	61.3	...	850	22	47.35	0.47	100.74	0.973	NO
HD015004.....	3973632	A0 III	198.0	...	280	4	31.33	0.31	101.06	1.302	YES	<35.88	11.96	3	13.64	UPL
HD015008.....	7345408	A1.5 V	41.5	...	405	5	178.77	1.44	124.15	0.983	NO	21.13	0.44	48.02	1.07	NO
HD015646.....	3973888	A0 V	118.1	...	260	4	19.59	0.2	97.95	1.008	NO	<10.25	3.42	3	4.875	UPL
HD016970.....	3974144	A3 V	25.1	Ursa Major	300	7	353.27	3.06	115.45	1.046	NO	45.29	4.75	9.53	1.223	NO
HD017254.....	11783424	A2 V	124.1	...	650	22	29.24	0.45	64.98	0.898	NO
HD018978.....	8794368	A4 V	26.4	...	350	5	240.39	2.63	91.4	1.03	NO	<26.56	8.86	3	1.054	UPL
	8794112															
HD019356.....	3974656	B8 V	28.5	...	300	8,5	1404.88	6.84	205.39	1.175	YES	206.23	11.79	17.49	1.586	YES
HD020315.....	3975168	B8 V	197.6	α Per	80	8	37.46	10.66	3.51	0.951	NO	<135.93	45.31	3	32.257	UPL
HD020888.....	11783680	A3 V	58.0	...	300	22	36.06	0.73	49.4	0.9	NO
HD021362 ^b	3976192	B6 Vn	169.8	α Per	80	8	313.31	3.66	85.6	8.201	YES	90.93	5.74	15.84	22.25	YES
HD021551.....	3976448	B8 V	266.7	α Per	80	8	27.61	1.04	26.55	0.958	NO	<61.37	20.46	3	20.103	UPL
HD021981.....	8812544	A1 V	113.5	...	265	5	39.15	0.8	48.94	0.86	NO
HD023267.....	3976960	A0 V	136.4	α Per	80	8	35.55	0.42	84.64	2.964	YES	<55.72	18.57	3	42.209	UPL
HD023642.....	3977984	A0 V	110.4	Pleiades	125	8	17.3	1.68	10.3	1.041	NO	<237.24	79.08	3	131.549	UPL
HD023753.....	3978240	B8 V	103.7	Pleiades	125	8	39.88	2.53	15.75	0.989	NO	<83.47	27.82	3	18.786	UPL
HD023763.....	3978496	A1 V	144.9	Pleiades	125	8	18.75	1.91	9.82	1.051	NO	<128.04	42.68	3	64.946	UPL
HD023862.....	3978752	B8 IVevar	118.8	Pleiades	125	8	662.14	6.4	103.46	8.986	YES	202.43	23.37	8.66	24.965	YES
HD023923.....	3979264	B8 V	116.6	Pleiades	125	8	46.21	0.89	51.92	1.749	YES	<118.80	39.6	3	40.679	UPL
HD023964.....	3975936	A0 V	158.7	Pleiades	125	8	17.15	0.25	68.6	0.974	NO	<8.00	2.67	3	4.23	UPL
HD025860.....	15421440	A4.5 IV	132.8	...	400	22	26.26	0.1	262.6	0.984	NO
HD026321.....	3979520	A0 V	175.1	α Per	80	8	13.48	0.11	122.55	0.976	NO	<12.2	4.07	3	7.945	UPL
HD027045.....	3979776	A3m	28.7	...	193	8,5	133.49	0.87	153.44	1.105	YES	45.73	7.03	6.5	3.406	YES
HD027628.....	3980032	A3m	45.7	Hyades	625	9	71.59	0.61	117.36	1.001	NO	<14.60	4.87	3	1.832	UPL
HD027749.....	3980288	A1m	47.2	Hyades	625	9	71.68	0.58	123.59	0.982	NO	<14.39	4.8	3	1.778	UPL
HD027962.....	3980544	A2 IV	45.4	Hyades	625	9,5	149.06	2.75	54.2	0.96	NO	<96.41	32.14	3	5.61	UPL
HD028226.....	3980800	Am	48.0	Hyades	625	9	72.96	1.02	71.53	1.051	NO	107.55	10.11	10.64	14.311	YES
HD028355.....	3981056	A7 V	49.2	Hyades	625	9,5	137.19	1.1	124.72	1.274	YES	178.78	5.45	32.8	15.389	YES
HD028527.....	3981312	A6 IV	44.4	Hyades	625	9,5	120.07	1.52	78.99	1.019	NO	37.36	5.94	3.83	2.94	YES
HD028546.....	3981568	Am	44.3	Hyades	625	9	75.31	0.46	163.72	1.026	NO	<15.38	5.13	3	1.947	UPL
HD029388.....	3981824	A6 V	45.9	Hyades	625	9,5	183.72	1.28	143.53	0.985	NO	<21.88	7.29	3	1.087	UPL
HD029488.....	3982080	A5 Vn	48.8	Hyades	625	9	139.51	0.51	273.55	0.987	NO	<13.36	4.45	3	0.875	UPL
HD030210.....	3982336	Am	81.7	Hyades	625	9	70.33	0.73	96.34	0.986	NO	<14.19	4.72	3.01	1.85	UPL

TABLE 1—Continued

Name	AOR Key	Spectral Type	Distance (pc)	Cluster/Moving Group	Age (Myr)	Age Reference	$F_{m,24}$ (mJy)	σ_{24} (mJy)	S/N ₂₄	R_{24}	IRE ₂₄	$F_{m,70}$ (mJy)	σ_{70} (mJy)	S/N ₇₀	R_{70}	IRE ₇₀
HD030422.....	3982592	A3 IV	57.5	...	10	3,5	44.67	0.64	69.8	1.202	YES	64.52	1.01	63.88	16.024	YES
HD031295.....	3982848	A0 V	37.0	...	10	3,5	167.25	1.94	86.21	1.25	YES	418.72	4.64	90.24	28.952	YES
HD033254.....	3983104	A2m	53.9	Hyades	625	9	72.62	1.39	52.24	1	NO	21.46	2.17	9.89	2.752	YES
HD034868.....	3983360	A0 V	136.8	...	300	4	25.9	0.3	86.33	0.983	NO	<21.68	7.23	3	7.658	UPL
HD038056.....	3983616	A0 V	132.5	...	250	4,5	36.48	0.37	98.59	1.823	YES	49.67	1.06	46.86	22.466	YES
HD038206.....	3983872	A0 V	69.2	...	9	4	106.92	1.58	67.67	3.361	YES	342.27	12.87	26.59	100.367	YES
HD038545.....	3984128	A3 Vn	129.5	...	13	4	45.89	0.72	63.74	0.979	NO	<13.6	4.53	3	2.678	UPL
HD038678.....	8792832	A2 Vann	21.5	...	231	8,5	860.2	17.2	50.01	2.598	YES	246.62	24.66	10	6.872	YES
	9798208															
HD039060.....	8970240	A5 V	19.3	β Pic	12	23,1,2	7276	728	9.99	23.015	YES	12990.4	1825.4	7.12	379.678	YES
	12613632															
HD040335.....	9192192	A0	112.7	...	5	5	18.11	0.48	37.73	0.919	NO
HD042525.....	13588224	A0 V	101.8	...	300	22	33.39	0.32	104.34	0.976	NO
HD043107.....	13476608	B8 V	84.9	...	80	5	56.18	1.1	51.07	0.961	NO
HD045557.....	3984640	A0 V	88.0	...	75	4	35.82	0.31	115.55	0.982	NO	<9.54	3.18	3	2.454	UPL
HD046190.....	9662976	A0 V	79.0	...	5	5	23.86	0.05	477.2	1.126	YES
HD047332.....	11892224	A1I V	343.6	...	400	22	16.41	0.28	58.61	1.019	NO
HD048915.....	9458432	A0 V	2.6	...	70	8,5	2535.26	17.81	142.35	0.926	NO
HD057336.....	13588736	A0 IV	384.6	...	400	10	10.05	0.18	55.83	0.957	NO
HD058142.....	7145472	A1 V	76.3	...	250	22	97.27	0.76	127.99	0.896	NO
HD058647 ^c	3985152	B9 IV	277.0	...	1	Ae/Be	2163.32	10.55	205.05	118.166	YES	267.78	3.03	88.38	131.912	YES
HD058715 ^b	3985408	B8 Ve	52.2	...	100	22,6	1469.42	7.75	189.6	3.413	YES	423.04	51.02	8.29	8.91	YES
HD065517.....	13589248	A2.5 IV	105.9	...	350	22	14.76	0.22	67.09	1.031	NO
HD069863.....	13589504	A2 V	74.2	...	650	5,11	81.78	3.6	22.72	1.014	NO
HD071043.....	3985664	A0 V	73.1	...	11	4	58.21	1.44	40.42	1.836	YES	97.22	29.12	3.34	28.442	YES
HD071155.....	3985920	A0 V	38.3	...	169	8,5	302.39	4.13	73.22	1.437	YES	211.74	2.76	76.72	9.087	YES
HD073210.....	3986432	A5 V	196.1	Praesepe	729	12	24.7	0.2	123.5	1.048	NO	<10.66	3.55	3	4.078	UPL
HD073666.....	3986688	A1 V	174.8	Praesepe	729	12	16.6	0.83	20	0.979	NO	<5.26	1.75	3.01	2.818	UPL
HD073731.....	3986944	A5m	168.1	Praesepe	729	12	30.05	0.51	58.92	0.942	NO	<6.78	2.26	3	1.973	UPL
HD073819.....	3987200	A6 Vn	183.2	Praesepe	729	12	21.03	0.19	110.68	1.008	NO	<6.13	2.04	3	2.732	UPL
HD073871.....	3987456	A0 III	160.5	Praesepe	729	12	19.26	0.09	214	0.984	NO	<6.76	2.25	3	3.231	UPL
HD074956.....	8794880	A1 V	24.4	...	390	8,5	1396.18	25.37	55.03	1.107	YES	<180.08	60.03	3	1.315	UPL
	8794624															
HD075416.....	3987712	B8 V	96.9	η Cha	8	23,13,14	122.44	1.29	94.91	3.273	YES	34.5	0.93	37.1	8.381	YES
HD076644.....	4239360	A7 V	14.6	...	620	5	629.55	4.1	153.55	1.028	NO	78.54	2.28	34.45	1.178	NO
HD079108.....	3987968	A0 V	115.2	...	320	4	44.98	1.16	38.78	1.791	YES	84.35	2.52	33.47	30.357	YES
HD080007.....	10091008	A2 IV	34.1	...	260	5	1768.9	4.54	389.63	1.006	NO	212.86	0.97	219.44	1.126	NO
HD080950.....	3988224	A0 V	80.8	...	80	4	114.67	1.53	74.95	3.5	YES	59.31	0.96	61.78	16.361	YES
HD082621.....	12398336	A2 V	81.9	...	285	5	127.75	0.85	150.29	0.979	NO	14.51	0.71	20.44	1.024	NO
HD083808.....	4231680	A5 V	41.5	...	400	5	816.76	1.28	638.09	0.984	NO	94.79	1.49	63.62	1.041	NO
HD087887.....	3988480	A0 III	88.1	...	295	4	108.94	0.27	403.48	0.983	NO	<9.81	3.27	3	0.811	UPL
HD087901.....	9661440	B7 V	23.8	...	140	5	1591.5	6.57	242.24	0.992	NO	179.25	35.85	5	1.034	NO
HD091375.....	9663232	A1 V	79.4	...	265	5	102.48	2.1	48.8	1.013	NO
HD092467.....	3988992	B9.5 V	141.2	IC2602	50	15	13.32	1.4	9.51	0.994	NO	<46.44	15.48	3	31.787	UPL
HD092536.....	3989248	B8 V	147.1	IC2602	50	15	46.19	0.55	83.98	2.507	YES	<60.76	20.25	3	30.078	UPL
HD092715.....	3989504	B9.5 V	130.7	IC2602	50	15	12.76	0.45	28.36	1.012	NO	<40.78	13.59	3	29.305	UPL
HD092783.....	3989760	B9 V	138.7	IC2602	50	15	13.39	0.37	36.19	0.99	NO	<64.45	21.48	3	43.523	UPL
HD092845.....	3990016	A0 V	185.5	...	300	4	40.64	0.84	48.38	0.952	NO	<11.05	3.68	3	2.392	UPL

TABLE 1—Continued

Name	AOR Key	Spectral Type	Distance (pc)	Cluster/Moving Group	Age (Myr)	Age Reference	$F_{m,24}$ (mJy)	σ_{24} (mJy)	S/N ₂₄	R_{24}	IRE ₂₄	$F_{m,70}$ (mJy)	σ_{70} (mJy)	S/N ₇₀	R_{70}	IRE ₇₀
HD093540.....	3990272	B6 V	143.1	IC2602	50	15	40.04	0.6	66.73	0.952	NO	<16.35	5.45	3	3.615	UPL
HD093549.....	3990528	B7 IV	131.6	IC2602	50	15	44.95	1.12	40.13	0.936	NO	<17.2	5.73	3	3.277	UPL
HD093738.....	3990784	B9.5 V	143.9	IC2602	50	15	23.87	1.38	17.3	1.149	NO ^d	<15.51	5.17	3	6.748	UPL
HD095418.....	7596800	A1 V	24.3	Ursa Major	300	7,8,5	1026.6	14.14	72.6	1.283	YES	421.13	84.23	5	4.849	YES
	7596288															
HD097585.....	3991040	A0 V	146.2	...	300	4	50.65	2.98	17	0.931	NO	<35.55	11.85	3	5.904	UPL
HD097633.....	3991296	A2 V	54.5	...	550	5	395.1	2.48	159.31	1.187	YES	75.17	1.88	39.98	2.092	YES
HD101452.....	15247104	A2	128.2	...	250	22	13.05	0.12	108.75	0.977	NO
HD102647.....	4314112	A3 V	11.1	...	50	8,5	1599.68	14.68	108.97	1.4	YES	676.47	45.54	14.85	5.421	YES
	4313856															
HD103287.....	3991552	A0 V	25.6	Ursa Major	300	7,8,5	788.49	7.37	106.99	0.987	NO	96.06	1.73	55.53	1.118	NO
HD105805.....	3991808	A4 Vn	94.3	Coma	500	16	38.09	0.46	82.8	0.947	NO	<8.69	2.9	3	1.963	UPL
HD106591.....	3992064	A3 V	25.0	Ursa Major	300	7,5	419.18	4.13	101.5	1.101	YES	65.45	3.79	17.27	1.601	YES
HD108382.....	3992320	A4 V	86.5	Coma	500	16	113.99	0.99	115.14	0.987	NO	26.87	1.23	21.85	2.122	YES
HD108767.....	3992576	B9.5 V	26.9	...	260	5	412.69	2.44	169.14	0.992	NO	49.26	1.9	25.93	1.107	NO
HD108945.....	3992832	A2pvar	95.3	Coma	500	16	55.18	0.92	59.98	0.976	NO	<27.78	9.26	3	4.574	UPL
HD109307.....	3993088	A4 Vm	106.3	Coma	500	16	26.69	0.51	52.33	0.933	NO	<6.98	2.33	3	2.235	UPL
HD110304.....	8811008	A1 IV	40.0	...	400	5,11	144.58	8.6	16.81	1.396	NO
HD110411.....	3993344	A0 V	36.9	...	10	3	139.88	1.21	115.6	1.517	YES	247.95	2.22	111.69	25.002	YES
HD111786.....	3993600	A0 III	60.2	...	200	3	66.01	1.1	60.01	1.314	YES	69.86	3.65	19.14	12.55	YES
HD112185.....	3993856	A0p	24.8	Ursa Major	300	7,5	1457.98	13.41	108.72	0.99	NO	178.35	4.2	42.46	1.1	NO
HD112413.....	3994112	A0spe	33.8	...	350	5	337.05	7.84	42.99	0.922	NO	40.27	1.75	23.01	1.032	NO
HD115892.....	3994368	A2 V	18.0	...	350	5	683.66	2.41	283.68	1.209	YES	96.62	6.47	14.93	1.593	YES
HD116706.....	3994624	A3 IV	78.0	Coma	500	16	40.88	0.65	62.89	0.945	NO	<10.25	3.42	3	2.211	UPL
HD116842.....	3714304	A6 Vn	24.9	Ursa Major	300	7	258.68	1.47	175.97	0.985	NO	33.42	3.68	9.08	1.156	NO
HD118878.....	3994880	A0 V	121.2	Upper Cen	15	14	20.19	0.33	61.18	0.96	NO	<7.01	2.34	3	3.051	UPL
HD123445.....	3995136	B9 V	218.8	UCen	15	14	18.96	0.54	35.11	0.963	NO	<12.91	4	3.23	6.14	UPL
HD125162.....	3995392	A0p	29.8	...	313	8,5	270.8	2.32	116.72	1.384	YES	364.67	3.88	93.99	17.225	YES
HD126135.....	3995648	B8 V	155.5	Upper Cen	15	14	22.49	1.7	13.23	2.008	YES	<34.54	11.51	3	27.998	UPL
HD126997.....	3995904	A0.5 V	144.5	Upper Cen	15	14	19.67	0.2	98.35	0.986	NO	<8.56	2.85	3	3.988	UPL
HD128207.....	3996160	B8 V	128.5	Upper Cen	15	14	30.99	0.67	46.25	1.139	YES	<11.65	3.88	3	3.908	UPL
HD128998.....	15247360	A1 V	131.4	...	250	22	32.05	0.28	114.46	0.983	NO
HD129655.....	15421696	A2	128.5	...	300	22	16.53	0.12	137.75	0.999	NO
HD130697.....	3996416	A2 V	128.2	Upper Cen	15	14	17.49	0.44	39.75	0.933	NO	<9.09	3.03	3	4.499	UPL
HD130841.....	6037760	A3 IV	23.7	...	495	5	785.59	3.59	218.83	0.979	NO	81.9	3.08	26.59	0.927	NO
HD132238.....	3996672	B8 V	191.9	Upper Cen	15	14	30.6	0.91	33.63	1.977	YES	<12.81	4.27	3	7.601	UPL
HD133880.....	3996928	B8 IV	126.6	Upper Cen	15	14	27.26	0.41	66.49	0.973	NO	<12.81	4.27	3	4.293	UPL
HD133937.....	3997184	B7 V	136.2	Upper Cen	15	14	23.09	0.23	100.39	0.959	NO	<11.25	3.75	3	4.332	UPL
HD135454.....	3997440	B9 V	137.2	Upper Cen	15	14	17.71	0.15	118.07	1.311	YES	<8.00	2.67	3	5.502	UPL
HD135742.....	3997696	B8 V	49.1	...	100	8,5	501.99	1.68	298.8	0.988	NO	71.5	8.37	8.54	1.322	NO
HD136246.....	3997952	A1 V	143.5	Upper Cen	15	14	14.93	0.22	67.86	1.288	YES	34.35	1.41	24.36	27.614	YES
HD136347.....	3998208	A0sp	123.5	Upper Cen	15	14	15.91	2.67	5.96	1.009	NO	<8.35	2.78	3	4.925	UPL
HD136482.....	3998464	B8.5 V	124.5	Upper Cen	15	14	42.11	0.3	140.37	2.966	YES	<20.91	6.97	3	13.485	UPL
HD137015.....	3998720	A2 V	146.6	Upper Cen	15	14	15.18	0.26	58.38	1.183	YES	<18.01	6	3	13.068	UPL
HD137919.....	3998976	B9 V	154.3	Upper Cen	15	14	21.04	6.1	3.45	1.141	NO ^d	<15.31	5.1	3	7.76	UPL
HD138923.....	3999232	B8 V	112.5	Upper Cen	15	14	58.05	0.37	156.89	2.854	YES	<17.21	5.74	3	7.675	UPL
HD139006.....	8793600	A0 V	22.9	...	314	8,5	1261.63	15.46	81.61	1.436	YES	542.03	80.7	6.72	5.633	YES
	8793344															

TABLE 1—Continued

Name	AOR Key	Spectral Type	Distance (pc)	Cluster/Moving Group	Age (Myr)	Age Reference	$F_{m,24}$ (mJy)	σ_{24} (mJy)	S/N ₂₄	R_{24}	IRE ₂₄	$F_{m,70}$ (mJy)	σ_{70} (mJy)	S/N ₇₀	R_{70}	IRE ₇₀
HD139160.....	3999488	B9 IV	184.2	Upper Sco	5	14	20.98	0.1	209.8	0.968	NO	<35.49	11.83	3	15.048	UPL
HD142703.....	3999744	A2 Ib/II	52.9	...	300	17	54.27	0.39	139.15	0.988	NO	<46.51	15.5	3	7.63	UPL
HD144661.....	4000256	B8 IV/V	117.6	Upper Sco	5	14	17.19	0.24	71.63	1.004	NO	<11.13	3.71	3	6.076	UPL
HD145964.....	4000768	B9 V	105.8	Upper Sco	5	14	19.01	1.6	11.88	0.95	NO	<15.72	5.24	3	7.248	UPL
HD158460.....	7970048	A1 V	104.4	...	260	5	53.15	0.34	156.32	1.155	YES	18.26	1.19	15.34	3.646	YES
HD158485.....	7969280	A4 V	109.3	...	420	5	24	0.1	240	0.94	NO
HD161868.....	8797184	A0 V	29.1	...	184	8,5	413.51	18.31	22.58	1.722	YES	1085.19	217	5	40.819	YES
	8796928															
HD163466.....	12872448	A2	196.5	...	310	5	20.15	0.13	155	0.958	NO
HD165459.....	9851392	A2 V	89.3	...	5	5	25.32	0.25	101.28	1.467	YES	25.93	1.08	24.01	13.664	YES
HD172167.....	9547776	A0 V	7.8	Castor	200	1,2	8900	89	100	1.12	YES	11416.1	2283.22	5	13.236	YE
	9458432															
HD172728.....	12872704	A0 V	130.5	...	210	5	31.33	0.15	208.87	0.918	NO
HD181296.....	8935424	A0 Vn	47.7	Tucana	30	23,18	382.43	6.46	59.2	5.186	YES	408.53	41.37	9.87	50.033	YES
	8935168															
HD183324.....	4002048	A0 V	59.0	...	10	3	50.3	1.25	40.24	1.114	YES	30.76	4.89	6.29	6.29	YES
HD188228.....	3725824	A0 V	32.5	...	10	8,5	170.75	0.55	310.45	0.977	NO	68.95	6.1	11.3	3.695	YES
HD193281.....	4002560	A2 III	218.3	...	600	3	27.26	1.93	14.12	1.01	NO	<7.96	2.65	3	2.649	UPL
HD198160.....	4002816	A2.5 IV/V	73.2	...	600	3	62.52	0.64	97.69	0.96	NO	62.07	5.78	10.74	8.609	YES
HD204041.....	4003328	A1 IV	87.3	...	400	3	33.54	0.37	90.65	1.124	YES	<8.78	2.93	3	2.647	UPL
HD209952.....	7979008	B7 IV	31.1	...	100	5	979.38	1.78	550.21	0.97	NO	120.77	0.71	170.1	1.129	NO
	7345152															
	9661696															
	13642240															
HD210049.....	3729920	A2 V	40.0	...	245	5	128.47	0.38	338.08	1.014	NO	<37.84	12.61	3	2.775	UPL
HD210111.....	4003584	A2 III/IV	78.7	...	700	3	36.59	1.25	29.27	0.979	NO	<9.46	3.15	3	2.264	UPL
HD210418.....	4003840	A2 V	29.6	...	450	5	336.71	3.32	101.42	0.994	NO	46.82	3.48	13.45	1.248	NO
HD213320.....	4004096	A0 IVs	81.4	...	300	4	71.85	0.85	84.53	1.005	NO	<12.24	4.08	3	1.6	UPL
HD214923.....	4004352	B8 V	63.9	...	120	5	241.91	2	120.96	0.977	NO	34.62	1.51	22.93	1.295	NO
HD215789.....	4004608	A3 V	39.7	...	470	5	363.17	2.37	153.24	1.007	NO	45.67	4.43	10.31	1.143	NO
HD216956.....	4889088	A3 V	7.7	Castor	200	1,2	3850	190	20.26	1.188	YES	9057.11	736.4	12.3	25.189	YES
	12582400															
HD216627.....	4004864	A3 V	48.9	Ursa Major	300	7,19	420.03	2.16	194.46	0.985	NO	54.7	7.12	7.68	1.18	NO
HD221756.....	4004608	A1 III	71.6	...	130	3	62.46	1.08	57.83	1.184	YES	41.52	2.68	15.49	7.283	YES
HD225200.....	3972608	A0 V	129.0	Blanco 1	90	20,21	34.7	0.7	49.57	1.495	YES	101.05	2.36	42.82	39.857	YES

NOTES.—Table 1 is also available in machine-readable form in the electronic edition of the *Astrophysical Journal*.

^a Age is set to 0 for the young stars that are below the ZAMS on the HRD.

^b Be stars.

^c Herbig Ae/Be star.

^d Stars are disregarded having 24 μm excess due to $\mathcal{X}_{24} < 3$.

REFERENCES.—(1) Barrado y Navascues 1998; (2) Song et al. 2000; (3) Pausen 1997; (4) Gerbaldi et al. 1999; (5) Rieke et al. 2005; (6) Westin 1985; (7) King et al. 2003; (8) Song et al. 2001; (9) Peryman et al. 1998; (10) Corbally & Gray 1996; (11) Corbally 1984; (12) Bonatto et al. 2004; (13) Mamajek et al. 2000; (14) de Zeeuw et al. 1999; (15) Randich et al. 2001; (16) Odenkirchen et al. 1998; (17) Iliev & Barzova 1995; (18) Zuckerman et al. 2001; (19) Eggen 1983; (20) Panagi & O'dell 1997; (21) Lynga & Wramdemark 1984; (22) this study; (23) Zuckerman & Song 2004.

TABLE 2
 INFORMATION ON THE ADDITIONAL *IRAS* STARS

Name	2MASS K_s (mag)	Age (Myr)	Spectral Type	F_{25} (Jy)	R_{25}	F_{60} (Jy)	R_{60}	$\sigma_{R_{60}}$	\mathcal{X}_{60}	Upper Limit
HD050241.....	2.62	660	A7 IV	0.891	0.993	0.230	1.48	0.31	1.54	2.10
HD005448.....	3.50	600	A5 V	0.395	0.994	0.118	1.71	0.46	1.54	2.63
HD033904.....	3.61	150	B9 IV	0.355	1.032	0.127	2.13	0.43	2.65	2.98
HD141003.....	3.31	300	A2 IV	0.439	0.964	0.177	2.24	0.54	2.31	3.31
HD027376.....	3.91	160	B9 V	0.247	0.947	0.103	2.27	0.52	2.44	3.32
HD130109.....	3.72	300	A0 V	0.353	1.088	0.125	2.22	0.55	2.20	3.33
HD077327.....	3.42	120	A1 Vne	0.478	1.165	0.161	2.26	0.56	2.23	3.39
HD080081.....	3.51	395	A3 V	0.393	1.042	0.151	2.31	0.58	2.27	3.46
HD056537.....	3.38	560	A3 V	0.586	1.320	0.177	2.30	0.60	2.17	3.49
HD118098.....	3.13	510	A3 V	0.550	0.986	0.236	2.44	0.54	2.68	3.51
HD079469.....	3.93	180	B9.5 V	0.332	1.296	0.109	2.45	0.61	2.37	3.68
HD153808.....	3.79	220	A0 V	0.289	0.991	0.139	2.74	0.58	3.03	3.90
HD088955.....	3.73	300	A2 V	0.356	1.154	0.148	2.76	0.77	2.28	4.31
HD198001.....	3.72	240	A1.5 V	0.318	1.023	0.155	2.87	0.78	2.41	4.42
HD089021.....	3.37	410	A2 IV	0.431	0.963	0.232	2.98	0.75	2.66	4.48
HD142105.....	4.12	180	A3 Vn	0.247	1.147	0.125	3.34	0.60	3.89	4.55
HD129246.....	3.64	320	A3 IVn	0.342	1.023	0.177	3.05	0.79	2.58	4.63
HD140436.....	3.77	160	B9 IV+	0.237	0.793	0.171	3.30	0.73	3.17	4.75
HD039014.....	3.70	540	A7 V	0.314	0.988	0.841	15.24	1.68	8.49	18.59

NOTES.— Reference for age used can be found in Rieke et al. (2005). Here, $\sigma_{R_{60}}$ is the error on the ratio (R_{60}) between measured flux and predicted flux based on $K_s - [24]$ color, \mathcal{X}_{60} is the significant of excess emission at $60 \mu\text{m}$, i.e., $(R_{60} - 1)/\sigma_{R_{60}}$, while the last column is a 2σ upper limit on R_{60} , i.e., $R_{60} + 2 \sigma_{R_{60}}$.

are logical members of our sample that have not been observed with *Spitzer* primarily because of the lack of accurate age estimates. Generally, the *Spitzer* programs emphasized young stars with ages estimated from membership in moving groups or clusters, while these unobserved stars tend to be relatively old according to ages estimated from their placement on the HRD (Rieke et al. 2005). We added them to this study using *IRAS* data to avoid any age bias. To do so, we proceeded as follows.

Given the large *IRAS* beams, we were concerned that noise associated with the background might produce false excesses. The background (IR cirrus) can be estimated either directly from models of the infrared sky (e.g., from the *Spitzer* Science Center SPOT user tool) or from the atomic hydrogen column, N_{H} (e.g., *Chandra* Colden: Galactic Neutral Hydrogen Density Calculator).⁶ We used both methods to guard against stars in high-cirrus regions; in general they gave consistent results. To determine a threshold for false excesses, we examined the $K_s - [25]$ colors of the full sample of stars as a function of the two background estimators. We concluded that stars with $N_{\text{H}} < 10 \text{ cm}^{-2}$ and IR background less than 1.3 MJy sr^{-1} at $60 \mu\text{m}$ are unlikely to suffer from cirrus confusion, and we trimmed the sample of 47 stars to 30 that meet both criteria. We next determined which of these stars have useful *IRAS* measurements at $60 \mu\text{m}$. We used the Faint Source Catalog (FSC) to obtain a $60 \mu\text{m}$ flux density measurement and an error in the measurement for each star. Most of the stars are not detected, but the errors allow us to set upper limits to their fluxes. We trimmed the sample to the 19 stars that have either detected excesses or excesses for which we could set 2σ upper limits at less than 5 times the photospheric flux density (Adopting 2σ limits allows meaningful limits in the same range as the *Spitzer* measurements, with a chance of one or two excesses slightly exceeding the actual limits for those 19 stars). Because the two cuts are based on sky properties, and then on *IRAS* signal-to-noise ratios, the remaining stars should be representative of the original sample that contained twice as many. The properties of these 19 stars are listed in

Table 2. The age distribution of the complete sample is shown in Figure 1.

3. PHOTOSPHERIC PREDICTION AND EXCESS DETERMINATION

3.1. Excess Identifications and Statistics

To determine the excess emission from the debris, the stellar contribution has to be subtracted from the measurements. We determined the stellar contribution at each band, using the best-fit synthetic Kurucz model (Castelli & Kurucz 2003) by fitting all available optical to near-infrared photometry (Johnson *UBVRJHK* photometry, Strömgen *uvby* photometry, *Hipparcos* Tyco *BV* photometry, 2MASS *JHK_s* photometry) based on a χ^2 goodness-of-fit test. For stars within 50 pc of the Sun, no correction for interstellar extinction was applied. For stars with distances larger than 50 pc, we estimated the extinction (A_V) based on the $B - V$ color and spectral type and then applied a reddening correction using the

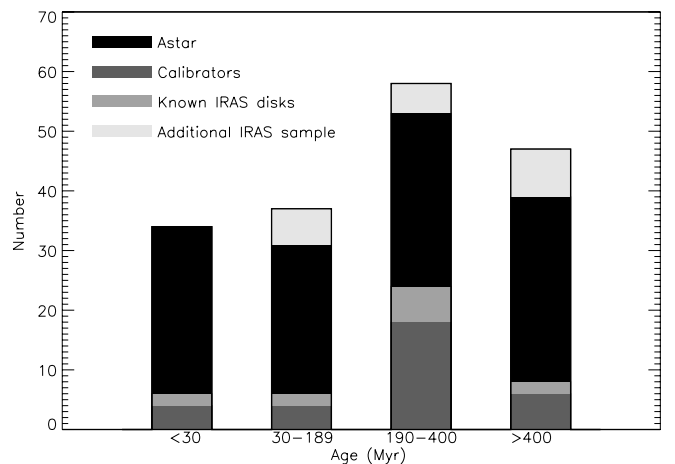


FIG. 1.—Age distribution of the complete sample.

⁶ See <http://cxc.harvard.edu/toolkit/colden.jsp>.

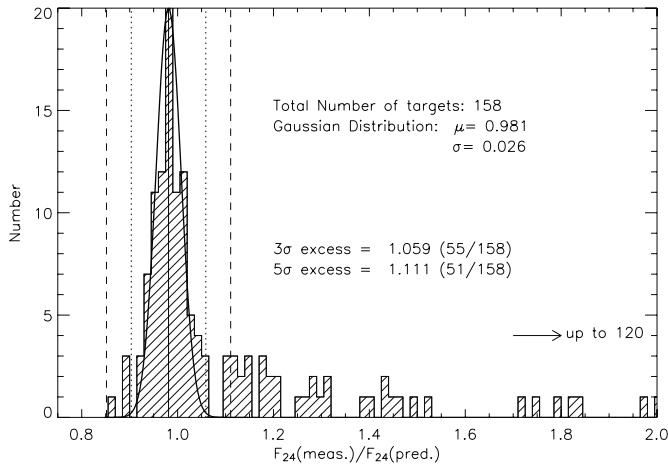


FIG. 2.—Distribution of the 24 μm fluxes relative to the expected photospheric values from the Kurucz model fittings. A Gaussian distribution with a dispersion of 0.026 is shown for comparison. Boundaries for $\pm 3\sigma$ (dotted lines) and $\pm 5\sigma$ (dashed lines) are marked. [See the electronic edition of the Journal for a color version of this figure.]

extinction curve from Cardelli et al. (1989). The predicted flux was then computed using the best-fit Kurucz model spectrum at the 24 and 70 μm weighted average wavelengths (23.68 and 71.42 μm , respectively).

To determine whether a star possesses a significant infrared excess, we first need to evaluate how good our photospheric predictions and measured photometry are. Figure 2 shows a histogram of the 24 μm fluxes ratioed to the expected photospheric values. A Gaussian distribution with a dispersion of 0.026 is shown for comparison and indicates that our predicted photospheres and measured photometry are as good as 2.6% at the 1 σ level. A few outliers with low flux ratio values are probably due to the effects of latent images (C. Engelbracht et al. 2006, in preparation). Note that the center of the Gaussian is at 0.981, suggesting a systematic offset of $\sim 2\%$. Based on this we define a 3 σ excess as a ratio greater than 1.06 or a 5 σ excess as a ratio greater than 1.11. There are four stars (HD 2266, HD 27045, HD 106591, and HD 74956) that have ratios between 3 and 5 σ , and three of them have confirmed 70 μm excesses (see below). Therefore, we adopt the ratio of 1.06 (3 σ excess) as our threshold for identifying infrared excesses at 24 μm .

A total of 137 stars have MIPS 70 μm observations, but only 69 stars have positive detections (signal-to-noise larger than 3). Figure 3 shows a histogram of the 70 μm fluxes relative to the expected photospheric values. A Gaussian distribution with a dispersion of 0.15 and centered at 1.11 is shown for comparison. The majority of the stars (40 out of 69) show large excesses ($>10\sigma$). We define a 3 σ excess as a ratio between measured and predicted fluxes greater than 1.55 and a 5 σ excess as a ratio greater than 1.84 at 70 μm . Four stars have ratios that fall between 3 and 5 σ excesses; and three of them (HD 19356, HD 106591, and HD 115892) have 24 μm excess above 3 σ (the exception is HD 4150). The 3 σ threshold at 70 μm is a consistent cutoff with the 3 σ threshold at 24 μm because none of the stars (a total of 22) that have ratios less than our 3 σ threshold at 70 μm has a 24 μm excess (more than 3 σ).

Using these criteria (3 σ excess as a flux ratio higher than 1.06 at 24 μm and 1.55 at 70 μm), each of the stars is then classified as “YES,” “NO,” or “UPL” in Table 1 (IRE₂₄ and IRE₇₀), corresponding to having an infrared excess, being detected but with no excess above the 3 σ confidence level, or having only an up-

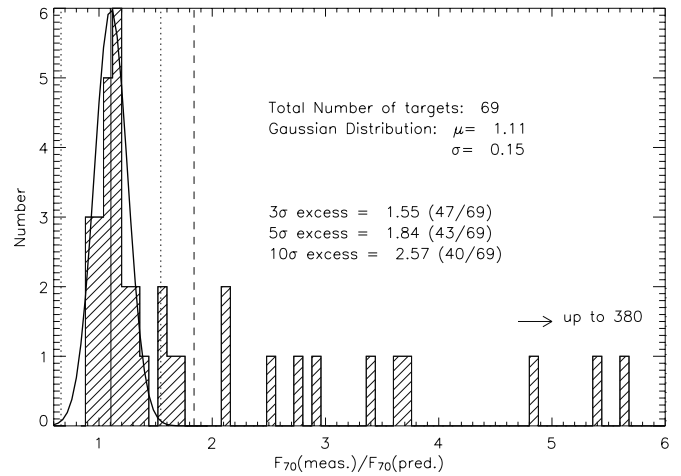


FIG. 3.—Distribution of the 70 μm fluxes relative to the expected photospheric values from the Kurucz model fittings. A Gaussian distribution with a dispersion of 0.15 is shown for comparison. Boundaries for $\pm 3\sigma$ (dotted lines) and $\pm 5\sigma$ (dashed lines) are marked. [See the electronic edition of the Journal for a color version of this figure.]

per limit. In addition, we also used the significance (\mathcal{X}) of a detected excess, defined as (measured – predicted)/uncertainty, for an internal check. At 70 μm , the excess stars identified by our flux ratio criterion all have $\mathcal{X}_{70} \geq 3$. At 24 μm , two stars (HD 93738 and HD 137919) have the excess significance \mathcal{X}_{24} less than 3, while the rest all have $\mathcal{X}_{24} \geq 3$. Unfortunately, the 70 μm measurements of these two stars are both upper limits and cannot verify the infrared excess nature of these two stars. We therefore regard HD 93738 and HD 137919 as having no 24 μm excesses.

At the 3 σ confidence level, the 24 μm excess rate is $32\% \pm 5\%$ out of 155 stars (three stars are not debris disks in nature, see § 4.1). If we assume that all the nondetected stars do not have 70 μm excesses, then the 70 μm excess rate is $33\% \pm 5\%$ (out of 134). This is a lower limit since in some cases the measured noise is much higher than the predicted photospheric flux. Therefore the excess rate at 70 μm could be as high as $67\% \pm 10\%$ (out of 66). Among the 44 stars that have excesses at 70 μm above the 3 σ confidence level, eight of them show no (less than 3 σ) 24 μm excess. These eight “only-70 μm ” excesses are unlikely to be false detections because the significance of the detected excesses are all greater than 4 at 70 μm (See Table 3, group II).

The fact that the excess rate at 24 μm and the lower-bound excess rate at 70 μm are similar indicates that MIPS 24 μm photometry is a very powerful and reliable tool for studying infrared excesses around early-type stars. Combining the 24 and 70 μm results, the infrared excess detection rate is at least $37\% \pm 5\%$ (58 out of 157) around A-type stars. Even using the same criteria ($R_{24} > \sim 1.2$ and $R_{70} > \sim 1.5$) for identifying excesses for the field (old) FGK stars ($12\% \pm 4\%$, Bryden et al. 2006) and M-type stars ($\sim 0\%$, Gautier et al. 2006), the excess detection rate around A-type stars ($\sim 30\%$, using the same thresholds) is considerably higher.

3.2. Decay Times

The distributions of 24 and 70 μm excesses with stellar age are illustrated in Figures 4 and 5. Twelve nearby debris disk stars discovered by *IRAS* are indicated by star-shaped symbols (for β Pic, Vega, and Fomalhaut) and plus signs (for HD 14055, HD 18978, HD 38678, HD 74956, HD 95418, HD 102647, HD 139006, HD 161868, and HD 181296). As has been found in Rieke et al. (2005) the amount of excess emission at 24 μm shows a rapid decline with stellar age ($\sim t_0/t$ and $t_0 \sim 150$ Myr), and a large variety

TABLE 3
DEBRIS DISK PROPERTIES

Name	$F_{\text{IRE},24}$ (mJy)	χ_{24}	$F_{\text{IRE},70}$ (mJy)	χ_{70}	$T_{[24]-[70]}$ (K)	f_d
Group I: 24 and 70 μm Excess Disks						
HD014055.....	87.06	13.1	766.18	4.9	75	6.71E-05
HD019356.....	209.51	30.6	76.21	6.5	219	3.19E-06
HD002262.....	18.06	4.5	47.81	12.8	98	7.07E-06
HD023862.....	588.46	91.9	194.32	8.3	235	3.14E-04
HD027045.....	12.69	14.6	32.3	4.6	99	1.05E-05
HD028355.....	29.51	26.8	167.16	30.7	82	5.59E-05
HD030422.....	7.5	11.7	60.49	59.9	76	4.86E-05
HD031295.....	33.49	17.3	404.26	87.1	71	4.46E-05
HD038056.....	16.47	44.5	47.46	44.8	96	4.81E-05
HD038206.....	75.11	47.5	338.86	26.3	86	1.36E-04
HD038678.....	529.07	30.8	210.73	8.6	206	9.75E-05
HD039060.....	6959.86	9.6	12956.2	7.1	108	1.42E-03
HD071043.....	26.51	18.4	93.8	3.2	91	4.74E-05
HD071155.....	91.95	22.3	188.44	68.3	105	2.51E-05
HD075416.....	85.03	65.9	30.38	32.7	221	4.74E-05
HD079108.....	19.87	17.1	81.57	32.4	88	4.97E-05
HD080950.....	81.9	53.5	55.68	58.0	154	7.48E-05
HD095418.....	226.4	16.0	334.27	4.0	116	1.27E-05
HD097633.....	62.37	25.1	39.24	20.9	160	7.09E-06
HD102647.....	457.38	31.2	551.69	12.1	123	1.99E-05
HD106591.....	38.37	9.3	24.58	6.5	159	4.95E-06
HD110411.....	47.66	39.4	238.03	107.2	84	3.69E-05
HD111786.....	15.79	14.4	64.29	17.6	88	2.95E-05
HD115892.....	118.24	49.1	35.96	5.6	250	1.13E-05
HD125162.....	75.08	32.4	343.5	88.5	86	5.06E-05
HD136246.....	3.34	15.2	33.11	23.5	73	4.78E-05
HD139006.....	383.07	24.8	445.81	5.5	125	1.43E-05
HD158460.....	7.12	20.9	13.25	11.1	108	5.26E-06
HD161868.....	173.41	9.5	1058.6	4.9	81	7.52E-05
HD165459.....	8.06	32.2	24.03	22.2	95	4.66E-05
HD172167.....	955.95	10.7	10553.6	4.6	72	2.33E-05
HD181296.....	308.69	47.8	400.36	9.7	120	1.97E-04
HD183324.....	5.13	4.1	25.87	5.3	84	1.04E-05
HD216956.....	608.31	3.2	8697.54	11.8	70	6.14E-05
HD221756.....	9.69	9.0	35.82	13.4	90	1.92E-05
HD225200.....	11.49	16.4	98.51	41.7	75	7.95E-05

Group II: Only 70 μm Excess Disks

HD004150.....	10.06	4.5	<119	<2.24E-06
HD011413.....	46.99	21.9	<66	<2.54E-05
HD028226.....	100.03	9.9	<60	<3.51E-05
HD028527.....	24.65	4.1	<83	<6.27E-06
HD033254.....	13.66	6.3	<93	<6.07E-06
HD108382.....	14.21	11.6	<85	<4.23E-06
HD188228.....	50.29	8.2	<61	<1.19E-05
HD198160.....	54.86	9.5	<61	<1.34E-05

Group III: Stellar Photospheres

HD015008.....	<249	<1.37E-06
HD016970.....	<114	<1.49E-06
HD076644.....	<170	<1.44E-06
HD080007.....	<361	<1.07E-06
HD082621.....	<141	<8.84E-07
HD083808.....	<125	<6.80E-07
HD087901.....	<83	<4.70E-07
HD103287.....	<322	<2.41E-06
HD108767.....	<146	<5.30E-07
HD112185.....	<244	<1.31E-06
HD112413.....	<341	<2.94E-06
HD116842.....	<99	<1.67E-06
HD130841.....	<140	<8.79E-07

TABLE 3—Continued

Name	$F_{\text{IRE},24}$ (mJy)	χ_{24}	$F_{\text{IRE},70}$ (mJy)	χ_{70}	$T_{[24]-[70]}$ (K)	f_d
Group I: 24 and 70 μm Excess Disks						
HD135742.....	<84	<4.10E-07
HD209952.....	<205	<9.16E-08
HD210418.....	<130	<1.57E-06
HD214923.....	<147	<4.21E-07
HD215789.....	<108	<1.40E-06
HD216627.....	<93	<1.61E-06

of excess amounts at any given age. The trend at 70 μm also shows a large variety at any given age in Figure 5. However, compared to the trend at 24 μm , the 70 μm excess trend has a much longer decay time with $t_0 \geq 400$ Myr.

We have carried out a simple analysis to show that the trends for different decay times at 24 and 70 μm evident in Figures 4 and 5 are statistically significant. We divided the sample into two parts, based on the 24 μm decay timescale of ~ 150 Myr (Rieke et al. 2005). Given the age uncertainties, we put the division at 400 Myr. For the stars with ages less than this value, we determined that the proportion of stars with excess ratios >1.3 at 24 μm and >5 at 70 μm were virtually identical (that is, 28 out of 109 and 26 out of 95, respectively). However, for the stars 400 Myr old or older, there were 0 stars out of 45 with excess ratios >1.3 at 24 μm , but 4 stars out of 38 with excess ratios >5 at 70 μm . We used the binomial theorem to show that the probability of these two results coming from the same parent distribution is only about 1%. That is, the 24 μm excesses decay more rapidly than those at 70 μm at the 99% confidence level.

4. DUST PROPERTIES AROUND A STAR DEBRIS DISKS

4.1. Circumstellar Gas Disks

Two stars in our sample, HD 21362 and HD 58715, are associated with the Be phenomenon, i.e., where the strong stellar wind from a fast rotating B-type star forms a circumstellar gas disk, showing hydrogen emission lines in the optical and excess radiation

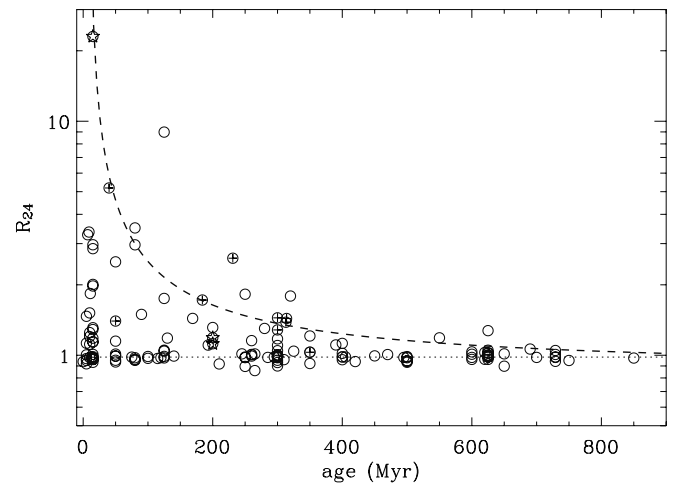


FIG. 4.—24 μm excess vs. age. Excess emission is indicated as the ratio of the observed flux density to that expected from the stellar photospheric value. β Pic, Vega, and Fomalhaut are additionally marked as star-shaped symbols, while stars from the IRAS-discovered debris disks are shown as plus signs. A decay curve of t_0/t is indicated as the dashed line, with $t_0 \sim 150$ Myr. [See the electronic edition of the Journal for a color version of this figure.]

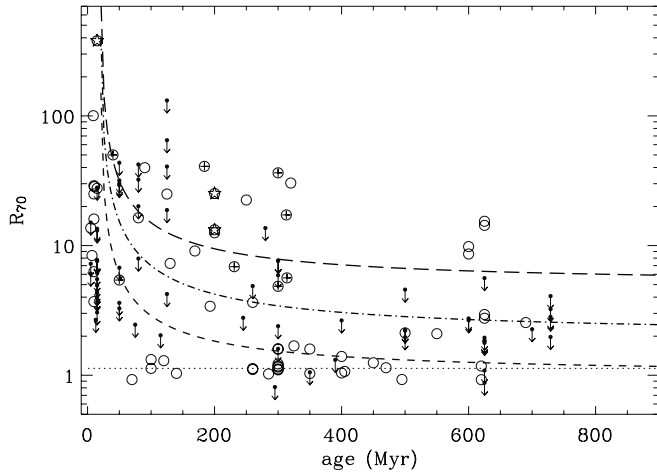


FIG. 5.— Similar to Fig. 4 but for 70 μm excess vs. age. The upper limits are shown in small dots with downward arrows. Three decay curves of t_0/t are indicated as the dashed line for $t_0 \sim 150$ Myr, the dot-dashed line for $t_0 \sim 400$ Myr, and the long-dashed line for $t_0 \sim 800$ Myr. [See the electronic edition of the *Journal* for a color version of this figure.]

relative to the expected photospheric flux in the infrared. The infrared excess emission is due to the free-free radiation from the ionized stellar wind. The nature of these gas disks can be recognized by several hydrogen lines seen in the IRS low resolution spectra (Fig. 6). The spectra were observed as part of the GTO follow-up debris disk programs. Details of the observations and data reduction will be discussed in an upcoming paper (K. Y. L. Su et al. 2006, in preparation). These two stars, as well as HD 58467 (a Herbig Ae/Be star), are not debris disks in nature, and are disregarded in the following discussion, as well as the preceding discussion on the infrared excess rates.

4.2. [24] – [70] Color Temperature

In the following sections, we discuss the dust properties in terms of the observed [24] – [70] color temperature and fractional dust luminosity with stellar age. There are 36 stars that have both 24

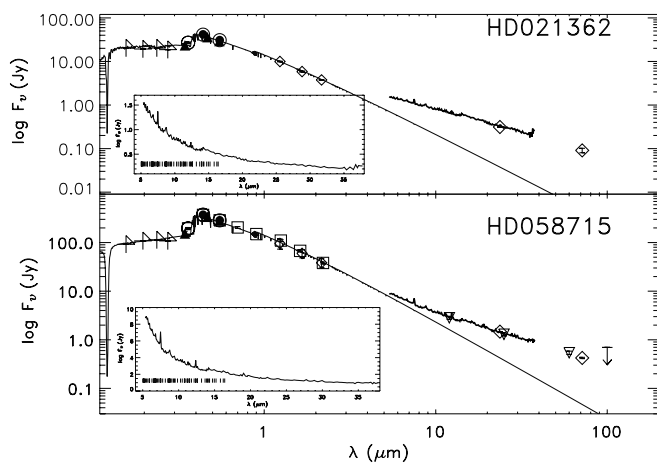


FIG. 6.— Spectral energy distributions for Be stars HD 21362 and HD 58715. Data plotted are TDI UV fluxes (*plus signs*), *uvby* photometry (*filled triangles*), Johnson *UBV* (*large open circles*), *Hipparcos* photometry (*small filled circles*), 2MASS photometry (*open diamonds*), *IRAS* color-corrected fluxes (*downward triangles* or *downward arrows* for upper limits), and MIPS fluxes (*open diamonds*). The IRS spectra are shown in gray lines between 5 and 38 μm , as well as in the small insets in a linear scale. The wavelengths of the hydrogen lines between 5 and 17 μm are identified in the small inset. The prominent line at 7.495 μm is the H α (18–8) line. [See the electronic edition of the *Journal* for a color version of this figure.]

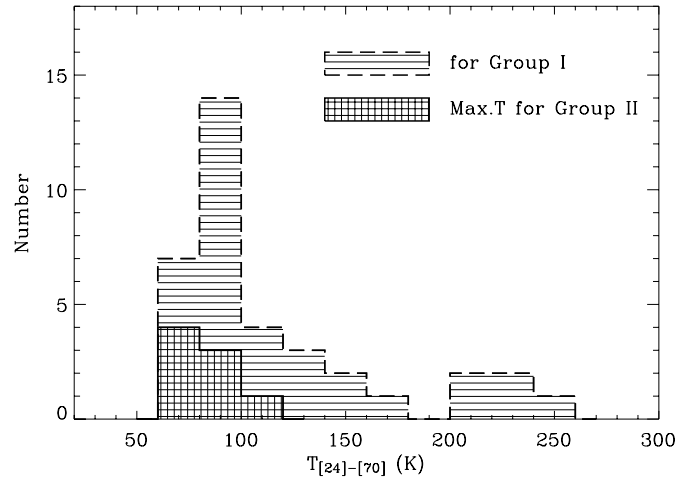


FIG. 7.— The [24 – 70] color temperature distribution of the disks. The stars that have both 24 and 70 μm excesses (group I) are displayed in a horizontal-lined pattern. The maximum color temperatures for stars in group II (only 70 μm excess) are shown in a mesh pattern.

and 70 μm excesses, above 3 σ confidence; hereafter, we refer to them as group I. The stars that only show 70 μm excess (a total of 8), we refer to as group II. Stars that have detections with S/N > 3 at both 24 and 70 μm but have no excess above the 3 σ levels, we refer to as group III (a total of 20). The infrared excess fluxes ($F_{\text{IRE},24}$ and $F_{\text{IRE},70}$ for 24 and 70 μm , respectively), significance of the excess fluxes (\mathcal{X}_{24} and \mathcal{X}_{70}), and the dust properties for stars from group I to III are listed in Table 3. Stars that have no significant 24 μm excesses and for which the 70 μm measurements are upper limits, we refer to as group IV (a total of 55). Group V (a total of 13) are the stars that have significant 24 μm excesses (above 3 σ confidence levels) but their 70 μm measurements are upper limits.

One simple way to characterize the disk properties based on the 24 and 70 μm excess emission is a blackbody fit to determine the color temperature ($T_{[24]-[70]}$) of the disk. It is straightforward to determine the color temperature for group I stars by ratioing the flux density at the two bands. Including the uncertainty in the excess fluxes, the color temperature generally has an uncertainty of ± 5 K for the group I stars. For the stars in group II (excess at 70 μm but not at 24 μm), a color temperature is computed by assuming that the excess flux at 24 μm is 3 times the measured uncertainty, which serves as a maximum temperature that the dust can have, consistent with our photometric accuracy. Figure 7 shows the color temperature histogram for the group I and group II stars.

The majority of the debris disks have $T_{[24]-[70]} \sim 90$ K, i.e., they are at a distance of ~ 100 AU from the star if we assume that the dust particles in these systems are blackbody-like. The Kuiper Belt in these A stars is expected to extend about 1.6 times farther than the Sun's (45–55 AU) following a simple mass scaling (Su et al. 2005). Hence, most of the debris around these A stars is Kuiper Belt-like if it consists of large (radius ≥ 50 μm) blackbody radiators. However, based on the study of the Vega debris disk (Su et al. 2005), non-blackbody-like small grains (radius ≤ 10 μm) can dominate the disk radiometric properties; therefore, the disk size can extend a few times larger if the dust grains in the system are small.

There are five stars that have [24] – [70] color temperatures larger than 200 K: HD 19356, HD 23862, HD 38678, HD 75416, and HD 115892. Since both HD 21362 and HD 58715 (gas disks) also have [24] – [70] color temperatures larger than 200 K, it is possible that these 5 stars are gas disks as well. However, no gas

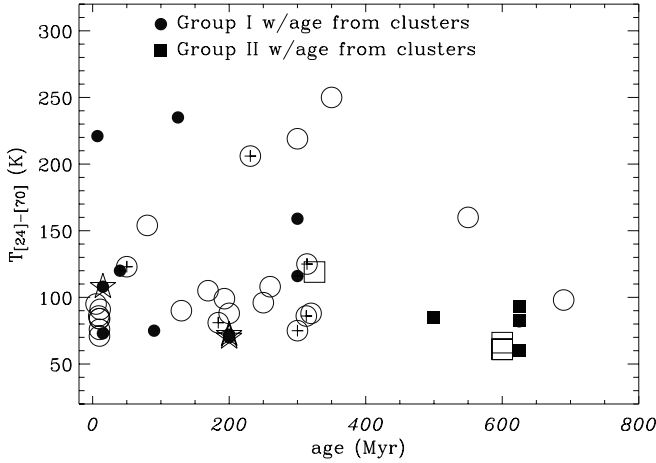


FIG. 8.—Stellar age vs. observed $[24] - [70]$ color temperature. Symbols used are circles for stars that have both 24 and 70 μm excess (group I), squares for stars only showing 70 μm excess (group II). Filled and smaller-sized symbols are for stars with age associated with clusters or moving groups. β Pic, Vega, and Fomalhaut are additionally marked as star-shaped symbols, while the stars from other *IRAS*-discovered disks are marked as plus signs. [See the electronic edition of the *Journal* for a color version of this figure.]

lines were seen in the mid-infrared spectra of HD 19356, HD 38678, and HD 115892 (Chen et al. 2006; K. Y. L. Su et al. 2006, in preparation), which leaves only HD 23862 and HD 75416 as possible gas disks.

Figure 8 shows the distribution of the observed $[24] - [70]$ color temperature with stellar age. Slightly smaller, but filled symbols represent the stars with ages determined from cluster associations. The ages determined from clusters or moving group association generally have errors less than 50%, but the ages determined from the HRD could have errors up to a factor of 2. It appears that the color temperature of the disks has a slightly broader distribution when stars are younger. For stars older than 400 Myr, most of the color temperatures of the disks appear in a narrow range between 50 and 150 K. Assuming the dust we see is blackbody-like (i.e., the location of the dust is directly related to dust temperature and stellar properties), the decrease of the $[24] - [70]$ color suggests that the debris is located farther away from the stars in the older systems, consistent with the significant difference in decay timescales between 24 and 70 μm , found in § 3.2.

4.3. Trends in Amounts of Excess Emission

Since the amounts of excess at both 24 and 70 μm decrease with stellar age (shown in § 3.2), it is important to have a large number of stars especially in the old age bin to ensure good statistics. As stated in § 2.3, an additional 19 A-type stars with *IRAS* observations at 25 and 60 μm were included to avoid an age bias. There are two candidates among these stars to show possible excesses at 25 μm : HD 56537, with a flux ratio of 1.32, and HD 79469, with a flux ratio of 1.30. Both are in the “marginal” category, since the deviations from unity flux ratio (no excess) are less than 3σ . There is only one star with a well-detected excess at 60 μm , HD 39014 (see, e.g., Jura et al. 2004). HD 142105 has a possible excess at 60 μm (3.9σ). For all the remaining stars, there are only upper limits at 60 μm . To analyze all the stars in this sample and in our *Spitzer* sample, in the following we will discuss 2σ upper limits for *IRAS* measurements at a uniform level of 1.25 at 25 μm and 5 at 60 μm .

These values correspond to a color temperature of ~ 90 K, which is typical of most of the debris systems (see Fig. 7). We divide stars from the *Spitzer* sample into those with measured ex-

TABLE 4
EXCESS AMOUNT VERSUS AGE

t (Myr)	Total No.	No Excess	Medium Excess	Large Excess
For 24/25 μm				
$t \leq 30$	34	20 (58%)	7 (21%)	7 (21%)
$30 < t \leq 189$	36	27 (75%)	5 (13%)	4 (11%)
$190 < t \leq 400$	59	50 (85%)	8 (14%)	1 (2%)
$400 < t$	45	44 (98%)	1 (2%)	0 (0%)
For 60/70 μm				
$t \leq 30$	31	16 (52%)	8 (25%)	7 (23%)
$30 < t \leq 189$	36	22 (62%)	7 (19%)	7 (19%)
$190 < t \leq 400$	46	34 (74%)	8 (17%)	4 (9%)
$400 < t$	40	35 (88%)	5 (12%)	0 (0%)

NOTE.—At 24 μm ($R_{24/25}$), No Excess = $R_{24} < 1.25$, Medium Excess = $1.25 \leq R_{24} \leq 2$, Large Excess = $R_{24} > 2$; at 70 μm ($R_{60/70}$), No Excess = $R_{70} < 5$, Medium Excess = $5 \leq R_{70} \leq 20$, Large Excess = $R_{70} > 20$.

cesses above these limits and those with excess or upper limits below them (i.e., $R_{24} > 1.25$ and $R_{70} > 5$ even with the 2σ upper limits). Combining the *IRAS* and *Spitzer* samples, a total of 174 stars were used at 24/25 μm , and 153 stars for 60/70 μm to study the trends in amounts of excess emission.

We further group the observations into bins in ages and amount of excess for three subgroups: “No” means no excess; “Large” means a flux ratio greater than 2 for 24 μm and 20 for 70 μm ; “Medium” means the flux ratio is intermediate. The age bins were set so that the total number of stars in each age bin is roughly equal.

The results are shown in Table 4 and Figure 9. The 24 μm excess trend is consistent with the results of Rieke et al. (2005) that $\sim 50\%$ – 60% of the stars that are younger than 30 Myr have no 24 μm excess, rising to $\sim 85\%$ – 95% for the stars that are older than 190 Myr. The trend of no excess at 70 μm is similar to 24 μm within the errors, but with a systematically lower fraction. The trends of infrared excess (either medium or large) are, again, similar, but the fractions at 70 μm are systematically higher than at 24 μm , suggesting that the rate of 70 μm excesses is higher than at 24 μm , and the persistence time of the 70 μm excess is longer;

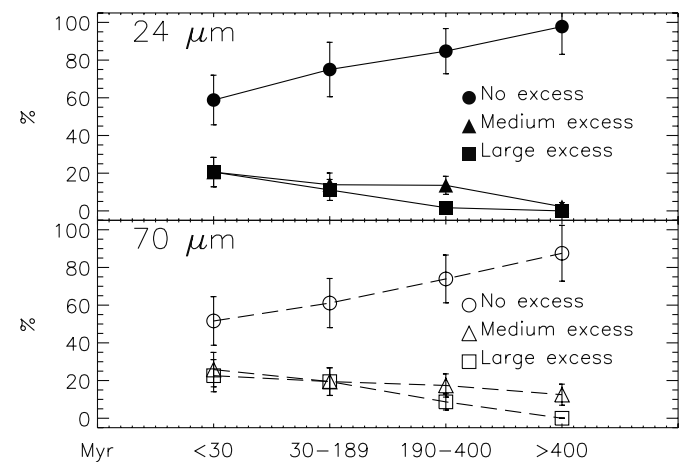


FIG. 9.—Trends of excesses with age at both 24 and 70 μm , based on Table 4. The 24 μm results are plotted as filled symbols with solid connecting lines, while the 70 μm results are plotted as open symbols with dashed connecting lines. No excess is shown in circles, Medium excess in triangles, and Large excess in squares. [See the electronic edition of the *Journal* for a color version of this figure.]

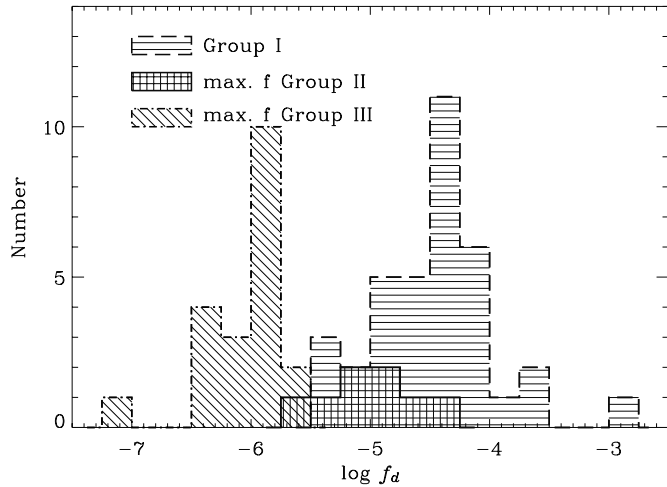


FIG. 10.—Fractional infrared luminosity distribution of the debris disks around A-type stars. The stars that have both 24 and 70 μm excesses (group I) are displayed in a horizontal-lined pattern, while the stars in group II (70 μm excess only) are in a mesh pattern. The group III distribution shows that our detection limits are strong enough that there should be no significant bias in the group I/II comparison. [See the electronic edition of the *Journal* for a color version of this figure.]

i.e., the debris primarily emitting at 70 μm remains in the system longer.

4.4. Fractional Dust Luminosity

The most frequently used quantity to measure the amount of dust in these systems is the fractional luminosity, f_d , the ratio of the total emission by dust to the stellar luminosity ($f_d = L_{\text{IR}}/L_*$). It measures the fraction of the sky seen from the star that is covered by dust, and therefore the fraction of the stellar radiation that will be absorbed and reemitted in the infrared (Dominik & Decin 2003). The fractional luminosity can be determined based on the observed [24] – [70] color temperature and an assumption of blackbody emission for the dust. However, the fractional luminosity estimated in this way is somewhat overestimated since the dust grains in the system probably have a $\lambda^{-\beta}$ emissivity dependence, where $\beta = 1-2$, and emit less efficiently at longer wavelengths than blackbody emission. The overestimate could be large, depending on details of the emissivity law. We discuss HD 225200 as an example in § 4.5; the fractional luminosity is $\sim 8\%$ overestimated between a blackbody and modified blackbody emission.

Large errors will result if these disks have substantial emission from cold (~ 30 K) dust. In most cases, there are no observations to constrain this possibility very well. However, examining the three best-studied nearby A-type debris disks, Vega, Fomalhaut, and β Pic, we find the flux ratio between 70 and 850 μm is ~ 140 , ~ 92 , and ~ 125 , respectively. Given the distinctly different properties of these three disks (age, fractional luminosity, and disk extent), an average flux ratio of ~ 120 between 70 and 850 μm should be representative for early-type debris disks. This average flux ratio gives a dust temperature of ~ 64 K assuming a $\beta = 1$ emissivity law, and the resultant fractional luminosity is roughly equal to or less than the one computed using the maximum color temperature. Applying similar logic, an upper limit fractional luminosity is also estimated for each of the stars in group III using a computed color temperature by assuming that the excess flux at each band is 3 times the measured uncertainty.

A histogram of fractional luminosity is shown in Figure 10. The majority of the stars have a fractional infrared luminosity $\sim 5 \times 10^{-5}$. Stars that only show 70 μm excess (group II) gen-

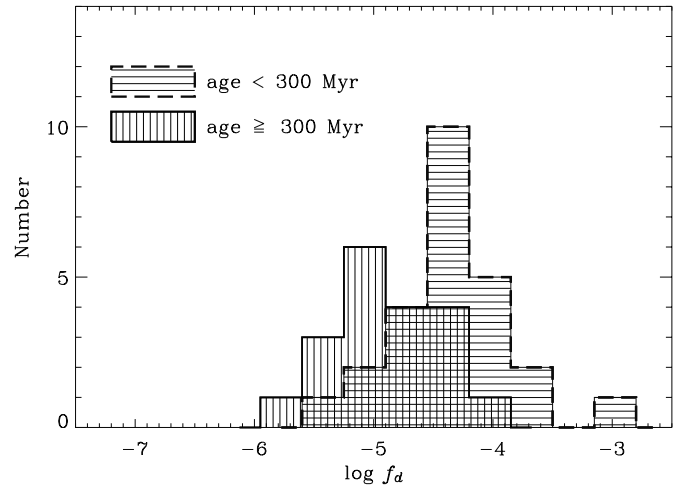


FIG. 11.—Same as Fig. 10, but with two age bins (older or younger than 300 Myr) among the group I and II stars. [See the electronic edition of the *Journal* for a color version of this figure.]

erally have lower fractional infrared luminosity. The maximum fractional luminosities for group III stars are much lower than the group I and II stars, consistent with their nondetectable infrared excess. To see the general trend of the fractional luminosity with age, we divide the group I and II stars into two age bins: older or younger than 300 Myr. This division is roughly at half the main-sequence lifetime of an A0 V star (the histogram is not sensitive to this age; it is similar if we make the cut at an age of 400 Myr). The fractional luminosity distribution for these two age groups is shown in Figure 11; older stars tend to have lower fractional luminosity than younger ones, which confirms the results from § 3.2 and Figure 9.

The distribution of the fractional luminosity with stellar age is shown in Figure 12. Several characteristics are found in this f_d versus age diagram:

1. The data are consistent with a general $1/t$ relation in the f_d versus age diagram but with at least 2 orders of magnitude variation in the amounts of f_d .

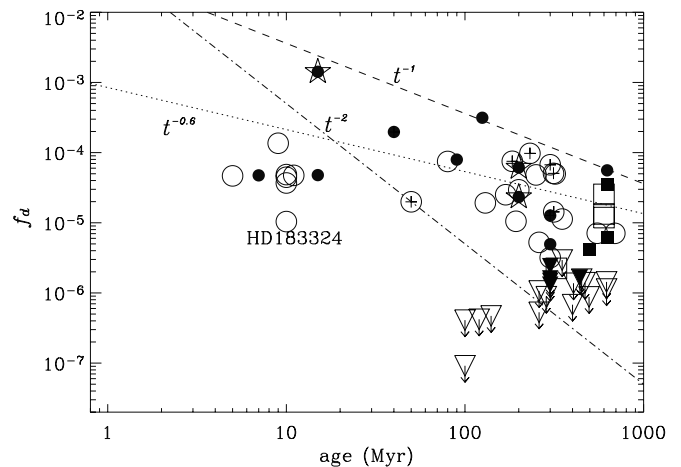


FIG. 12.—Stellar age vs. fractional luminosity. Symbols are as in Fig. 8. Additional data points from group III stars (maximum detectable fractional luminosity) are shown as upside-down triangles with arrows pointing downward, indicating our detection limits. The $1/t$ relation is shown as a dashed line, while the $1/t^2$ is shown as a dot-dashed line, with arbitrary normalization. A $1/t^{0.6}$ relation was obtained by fitting all the confirmed excess stars (group I and II), shown as a dotted line. [See the electronic edition of the *Journal* for a color version of this figure.]

2. An upper envelope of $1/t$ is seen in Figure 12. We do not detect any stars that are older than 100 Myr and have f_d values greater than 10^{-3} in this early-type sample.

3. All the only-70 μm excess stars (group II, squares in Fig. 12) are old. No stars that are younger than 100 Myr have only-70 μm excess. This trend could result from sample selection bias, because most of the young stars are at larger distances, and only 70 μm upper limits were obtained. Among the 53 group IV stars (no 24 μm excess and 70 μm is an upper limit), 6 are younger than 100 Myr, have 3σ upper limit ratios larger than 5, and, most importantly, have clean backgrounds based on the 24 μm images. These 6 stars are potential only-70 μm excess young stars. Future deeper 70 μm observations can help to better identify their natures.

4. Stars that have no detectable excess (group III, upside down triangles with downward arrows in Fig. 12) have f_d as low as $\sim 10^{-7}$ (similar to the value in our solar system).

A constant upper envelope of $f_d \approx 10^{-3}$ is suggested by Decin et al. (2003) based on a reanalysis of the data obtained with ISOPHOT and revised age estimates. This upper constant cutoff is not seen in these new *Spitzer* observations (item 2). Although Decin et al. combine all the available spectral types on the same plot, it is possible that the maximum fractional luminosity is different for different spectral types.

Dominik & Decin (2003) suggest that the total disk mass in a system and the location and sizes of the parent bodies are the three major parameters in determining the place in the f_d versus age diagram. They conclude that a $1/t$ relation indicates the dust removal process is dominated by collisions, and that Poynting-Robertson (P-R) drag would yield a $1/t^2$ relation. Collisions that result in small grains that are blown out of the system via radiation pressure are the dominant mechanism for removing dust in the bright debris disk systems observed by *IRAS* and *ISO*. This is true for these early-type stars since blowout occurs for grains $\lesssim 10 \mu\text{m}$; however, radiation pressure from lower luminosity stars (late K and M dwarfs) may not be adequate to remove any grains at all, and stellar wind drag is the dominant mechanism for removing grains in the young late K to M dwarfs (Plavchan et al. 2005). Hence, for the A-G systems, P-R drag only plays an important role when the density of the debris is as low as in our solar system (Dominik & Decin 2003; Wyatt 2005). Therefore, most (if not all) of the stars in the f_d versus age diagram should follow a $1/t$ trend. This is consistent with what we see in these new *Spitzer* data.

Assuming that the group IV stars have no 70 μm excess as well, the true lower envelope in the f_d versus age diagram is then very low. The total surface area occupied by dust may be greatly enhanced by collisions, and then follow a $1/t$ steady state collisional cascade. If the only-70 μm excesses are, indeed, only found associated with older stars, it means that the clearing process (collisions) is an inside out process. The collision frequency is higher closer to the stars because of larger relative velocities; therefore, the dust will be ground down to finer debris (subject to radiation blowout) faster. This is consistent with what Wyatt (2005) has suggested.

Alternatively, the “clearing” of the inner region could also arise from the decline of inward grain transport, rather than the removal of the initial inner-disk grain population. A secular decline in the collision rate in the outer disk might account for a drop in inward grain transport, and thus a drop in 24 μm emission with time. A crucial question for this model is whether the particles generated at the 70 μm emission zone (50–200 AU for A stars) have enough time to drift inward before they get destroyed by collisions. Assuming an A-type star of $2.5 M_\odot$ and $60 L_\odot$ with a debris disk of $f_d \sim 5 \times 10^{-5}$, the P-R lifetime ($\sim 10^7$ – 10^8 yr) is roughly 100 times the collisional lifetime ($\sim 10^5$ – 10^6 yr) for grains with

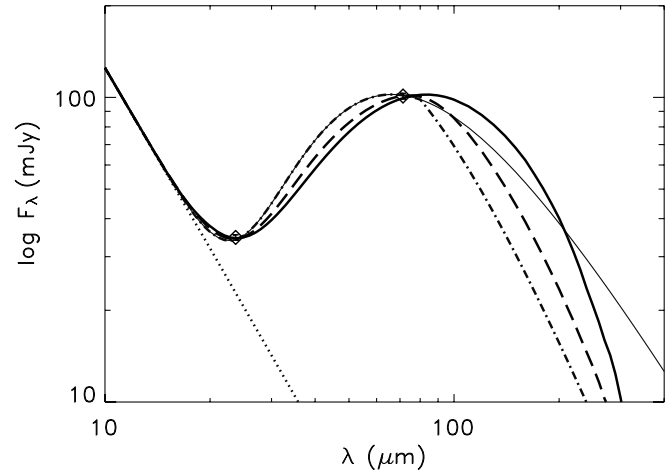


FIG. 13.—Model SEDs for HD 225200. The dotted line represents the stellar photosphere. The solid line is the SED assuming blackbody emission at $T_d = 75$ K, while the dash-dotted line assumes a modified blackbody emission $(\lambda/\lambda_0)^{-1} B_\nu(75 \text{ K})$ with $\lambda_0 = 80 \mu\text{m}$. The long dashed line is the best-fit SED using KBO-like grains, while the dash-triple-dotted line is the best-fit SED using Vega-like grains. Both models go through the 24 and 70 μm points, but have noticeably different shapes between these points. [See the electronic edition of the *Journal* for a color version of this figure.]

radii $\sim 100 \mu\text{m}$ and density of 2.5 g cm^{-3} at distances of 50–200 AU from the star. Therefore, the population of the particles that drift inward from the 70 μm zone to the 24 μm emission zone is likely to be small. Furthermore, we do not expect the color temperature to evolve with time if the 24 μm emission comes from material that is spiraling in from the colder, outer disk via P-R drag. The amount of the dust we see in these systems suggests that the dominant particle removal mechanism is collisions. P-R drag may only be important for older systems, as it does not explain the dust temperature trend seen in the systems from 5 to 850 Myr of age.

4.5. Debris Disk Model: Vega-like Grains or KBO-like Grains

As has been thoroughly discussed in the literature, debris disk modeling based on the broadband spectral energy distribution (SED) alone is degenerate, and hence not conclusive in constraining the debris distribution or dust properties. Based on the resolved disk surface brightness profiles (100–800 AU), Su et al. (2005) have shown that the majority of the dust particles in the disk are small grains in the prototype Vega debris disk. In comparison, the Vega SED has been modeled using large 30–200 μm grains in a ringlike (80–120 AU) disk (Dent et al. 2000). Resolving the disk extent is important. Unfortunately most of the debris disks we discuss here are not resolved with *Spitzer*’s beams. Without further constraints, there are many degeneracies using two data points (24 and 70 μm) to constrain a (at least) six-parameter disk model (surface density power-law index p , grain size power-law index q , grain size limits [a_{min} to a_{max}], and disk extent [R_{in} to R_{out}]).

As an illustration, we fit the observed SED of HD 225200 with two different predetermined models, Vega-like or KBO-like, using astronomical silicate grains. In the Vega-like model, we restrict the grains to be “small” (i.e., $a_{\text{min}} \sim 1 \mu\text{m}$, $a_{\text{max}} < 50 \mu\text{m}$, and $q = -2.5$) and to be driven outward by radiation pressure; therefore, $p = 1$. In the KBO-like model, we restrict the grains to be “large” (i.e., $a_{\text{min}} \sim 10 \mu\text{m}$, $a_{\text{max}} = 100 \mu\text{m}$, and $q = -3.5$), and to spiral inward due to the P-R drag; therefore, $p = 0$. The remaining two parameters to fit are R_{in} and R_{out} .

We searched large regions of parameter space, computing a χ^2 statistic at each point. At 90% confidence, we find that $R_{\text{in}} = 35 \pm 15$ AU, $R_{\text{out}} = 120 \pm 117$ AU with dust mass of $8.5 \pm 4.3 \times 10^{-3} M_{\oplus}$ for the KBO-like model, and $R_{\text{in}} = 100 \pm 55$ AU, $R_{\text{out}} = 900 \pm 450$ AU with dust mass of $21.40 \pm 5.2 \times 10^{-3} M_{\oplus}$ for the Vega-like model. Figure 13 shows the resulting SEDs. The outer radius in the Vega-like model (~ 900 AU, $\sim 7''$ given a distance of 129 pc) is theoretically resolvable with MIPS at $24 \mu\text{m}$. The fact that our shallow $24 \mu\text{m}$ observation indicates HD 225200 to be an unresolved point source indicates either that deeper imaging might be required to detect the disk outer boundary or that Vega-like grains are not likely present in the system. Furthermore, the two models yield different amounts of emission at wavelengths greater than $\sim 100 \mu\text{m}$. Without resolved images, data points at far-infrared and submillimeter wavelengths can provide further constraints on the disk outer boundary. Follow-up IRS observations of these A-type debris disks can also put additional constraints on the disk model (inner radius and grain sizes) and will be addressed in another paper.

5. SUMMARY AND CONCLUSION

About 160 A-type main-sequence stars with ages ranging from 5 to 850 Myr were measured at 24 and/or $70 \mu\text{m}$ using the Multiband Imaging Photometer for *Spitzer*. With *Spitzer*'s unprecedented sensitivity, we are able to identify infrared excesses of $\sim 6\%$ at $24 \mu\text{m}$ and $\sim 55\%$ at $70 \mu\text{m}$ above the photospheres at the 3σ levels. At this 3σ confidence level, the infrared excess rate is $32\% \pm 5\%$ and $\geq 33\% \pm 5\%$ for 24 and $70 \mu\text{m}$, respectively. The excess detection rate around these early-type stars is significantly higher than the one found in the old FGK (Bryden et al. 2006) and M-type stars (Gautier et al. 2006). However, recent studies by Gorlova et al. (2006) and Siegler et al. (2006) show that the excess rate for young FGK stars is also higher than for old FGK stars; most importantly, the evolution in the trend of excess rate versus age looks similar between A stars and FGK stars (only the absolute fraction is different) in their studies. Is there an intrinsic difference in the infrared excess rates between A-type and FGK stars? This is not an easy question to answer because equivalent levels of fractional luminosity become increasingly hard to detect as the star becomes cooler. The incidence of debris disks is actually the convolution of how many stars actually possess debris disks with given properties and how detectable the disks are with *Spitzer*, and this convolution is a strong function of spectral type. Thus, debris disk excess emission is not a steep

function of stellar type. Since the detectability of a given level of fractional excess decreases with decreasing stellar temperature, the incidence of excesses is consistent with similar debris disk driven fractional excesses between A and K stars. Nevertheless, it appears that age is the most important factor in determining the detectability of infrared excess among A- to K-type main-sequence stars, not stellar mass.

The amount of excess emission decreases with stellar age and follows a simple t_0/t relationship, in general, with $t_0 \sim 150$ Myr for excesses at $24 \mu\text{m}$ but $t_0 \geq 400$ Myr at $70 \mu\text{m}$; that is, $24 \mu\text{m}$ excesses decay more rapidly than those at $70 \mu\text{m}$. In addition, at any given age there exists a large variety in the amount of 24 and $70 \mu\text{m}$ excess emission. The observed $[24] - [70]$ color temperatures for a total of 44 debris disks with 24 and/or $70 \mu\text{m}$ excesses range from ~ 60 to ~ 250 K, but the majority of the disks have a typical temperature of ~ 90 K. Furthermore, older stars (age > 300 Myr) tend to have colder observed $[24] - [70]$ color temperatures than young ones. Assuming the dust we detect is blackbody-like, the decline of the $[24] - [70]$ color implies that the debris is located farther away from the stars in the older systems.

The fractional luminosity for these 44 early-type debris disks ranges from $\sim 10^{-3}$ to $\sim 10^{-6}$. The trend between the fractional luminosity and stellar age follows a general $1/t$ relationship; older stars tend to have lower fractional luminosity than younger ones. An upper envelope of $1/t$ is seen in the fractional luminosity versus age diagram, suggesting that collisions followed by radiation pressure blowing out small grains are the dominant process to remove grains in these systems. The decreases of observed $[24] - [70]$ color temperatures and the fractional luminosity suggest that the debris disk clearing is an inside out process.

Based on observations with NASA *Spitzer* Space Telescope, which is operated by the Jet Propulsion Laboratory, California Institute of Technology under NASA contract 1407. Support for this work was provided by NASA through Contract Number 1255094 issued by JPL/Caltech. This research made use of the SIMBAD database, operated at CDS, Strasbourg, France. This publication makes use of data products from the Two Micron All Sky Survey, which is a joint project of the University of Massachusetts and the Infrared Processing and Analysis Center/California Institute of Technology, funded by the National Aeronautics and Space Administration and the National Science Foundation.

REFERENCES

- Barrado y Navascues, D. 1998, *A&A*, 339, 831
 Bonatto, C., Bica, E., & Girardi, L. 2004, *A&A*, 415, 571
 Bryden, G., et al. 2006, *ApJ*, 636, 1098
 Cardelli, J. A., Clayton, G. C., & Mathis, J. S. 1989, *ApJ*, 345, 245
 Castelli, F., & Kurucz, R. L. 2003, in *Poster Papers, IAU Symp. 210: Modelling of Stellar Atmospheres*, ed. N. Piskunov, W. W. Weiss, & D. F. Gray (San Francisco: ASP), 20
 Chambers, J. E. 2004, *Earth Planet. Sci. Lett.*, 223, 241
 Chen, C. H., et al. 2006, *ApJS*, 166, 351
 Corbally, C. J. 1984, *ApJ*, 285, 195
 Corbally, C. J., & Gray, R. O. 1996, *AJ*, 112, 2286
 Decin, G., Dominik, C., Waters, L. B. F. M., & Waelkens, C. 2003, *ApJ*, 598, 636
 Dent, W. R. F., Walker, H. J., Holland, W. S., & Greaves, J. S. 2000, *MNRAS*, 314, 702
 de Zeeuw, P. T., Hoogerwerf, R., de Bruijne, J. H. J., Brown, A. G. A., & Blaauw, A. 1999, *AJ*, 117, 354
 Diolaiti, E., Bendinelli, O., Bonaccini, D., Close, L., Currie, D., & Parmegiani, G. 2000, *A&AS*, 147, 335
 Dominik, C., & Decin, G. 2003, *ApJ*, 598, 626
 Eggen, O. J. 1983, *AJ*, 88, 642
 Gautier, T. N., III, Rieke, G. H. Stansberry, J. A., Bryden, G. C., Stapelfeldt, K. R., Werner, M. W., Beichman, C. A., Chen, C. H., Su, K. Y. L., Trilling, D., Patten, B., & Roellig, T. 2006, *ApJ*, submitted
 Gerbaldi, M., Faraggiana, R., Burnage, R., Delmas, F., Gómez, A. E., & Grenier, S. 1999, *A&AS*, 137, 273
 Gomes, R., Levison, H. F., Tsiganis, K., & Morbidelli, A. 2005, *Nature*, 435, 466
 Gordon, K. D., et al. 2005, *PASP*, 117, 503
 Gorlova, N., Rieke, G. H., Muzerolle, J., Stauffer, J. R., Siegler, N., Young, E. T., & Stansberry, J. H. 2006, *ApJ*, 649, 1028
 Habing, H. J., et al. 2001, *A&A*, 365, 545
 Iliev, I. K., & Barzova, I. S. 1995, *A&A*, 302, 735
 Jura, M., et al. 2004, *ApJS*, 154, 453
 King, J. R., Villarreal, A. R., Soderblom, D. R., Gulliver, A. F., & Adelman, S. J. 2003, *AJ*, 125, 1980
 Kleine, T., Munker, C., Mezger, K., & Palme, H. 2002, *Nature*, 418, 952
 Krist, J. 2002, *Tiny Tim/SIRTF User's Guide* (Pasadena: SSC)
 Lynga, G., & Wramdemark, S. 1984, *A&A*, 132, 58
 Mamajek, E. E., Lawson, W. A., & Feigelson, E. D. 2000, *ApJ*, 544, 356
 Odenkirchen, M., Soubiran, C., & Colin, J. 1998, *NewA*, 3, 583
 Panagi, P. M., & O'dell, M. A. 1997, *A&AS*, 121, 213
 Panuzen, E. 1997, *A&A*, 326, L29

- Perryman, M. A. C., et al. 1998, *A&A*, 331, 81
- Plavchan, P., Jura, M., & Lipsy, S. J. 2005, *ApJ*, 631, 1161
- Randich, S., Pallavicini, R., Meola, G., Stauffer, J. R., & Balachandran, S. C. 2001, *A&A*, 372, 862
- . 2005, *ApJ*, 620, 1010
- Siegler, N., Muzerolle, J., Young, E. T., Rieke, G. H., Mamajek, E. E., Trilling, D. E., Gorlova, N., & Su, K. Y. L. 2006, *ApJ*, in press
- Song, I., Caillault, J.-P., Barrado y Navascués, D., & Stauffer, J. R. 2001, *ApJ*, 546, 352
- Song, I., Caillault, J.-P., Barrado y Navascués, D., Stauffer, J. R., & Randich, S. 2000, *ApJ*, 533, L41
- Spangler, C., Sargent, A. I., Silverstone, M. D., Becklin, E. E., & Zuckerman, B. 2001, *ApJ*, 555, 932
- Strom, R. G., Malhotra, R., Ito, T., Yoshida, F., & Kring, D. A. 2005, *Science*, 309, 1847
- Su, K. Y. L., et al. 2005, *ApJ*, 628, 487
- Westin, T. N. G. 1985, *A&AS*, 60, 99
- Wyatt, M. C. 2005, *A&A*, 433, 1007
- Zuckerman, B., & Song, I. 2004, *ARA&A*, 42, 685
- Zuckerman, B., Song, I., & Webb, R. A. 2001, *ApJ*, 559, 388